CHEMISTRY OF MATERIALS

pubs.acs.org/cm

Article

Influence of Stacking on H^+ Intercalation in Layered $ACoO_2$ (A = Li, Na) Cathode Materials and Implications for Aqueous Li-Ion Batteries: A First-Principles Investigation

Sergio Posada-Pérez, Gian-Marco Rignanese, and Geoffroy Hautier*

Cite This: *Chem. Mater.* 2021, 33, 6942−6954

Read Online

ACCESS | Metrics & More | Article Recommendations | Supporting Information

ABSTRACT: Li- and Na-ion batteries are effective energy storage technologies. Nonetheless, currently used organic-electrolyte batteries present well-known safety problems. Therefore, the research community is intensively looking for potential alternatives. Aqueous batteries based on low-cost salts in water could be an interesting choice since they are safe and environmentally benign. However, working with aqueous electrolytes brings new detrimental mechanisms such as proton intercalation. Understanding the (de)intercalation chemistry of protons and alkali is one of the keys for designing cathode materials in such aqueous electrochemical cells. In this work, we carry out density functional theory calculations to investigate the H^+/alkali exchange in layered $LiCoO_2$ and $NaCoO_2$ materials. By computing the grand potential phase diagram and voltage−composition plots, we determine the relative stability of several orderings of protons, alkali, and vacancies. The fully protonated CoO_2 lattice (CoO(OH)) is revealed to be the most stable insertion product due to the formation of interlayer hydrogen bonds. Our computations demonstrate the key role of layer stacking: H^+ insertion is favored in prismatic (P) stacking, while Li favors octahedral (O) stacking. While the fully protonated layered cobalt oxide is the thermodynamically favored product when protons and alkali compete, we show that mixing protons and lithium is energetically disfavored because of the different stacking preferences. We suggest that the kinetic difficulty in nucleating fully protonated phases in the layered oxide prevents proton insertion when cycling $LiCoO_2$ in an aqueous electrolyte. The good cyclability and lack of proton insertion in $LiCoO_2$ are, therefore, a result of the slow kinetics of protonation in partially lithiated cobalt oxide. On the other hand, we demonstrate that $NaCoO_2$ is prone to proton and alkali mixing due to the different stacking preferences for sodium. We hypothesize that this could lead to proton intercalation and poor performances in aqueous batteries for $NaCoO_2$ cathodes.

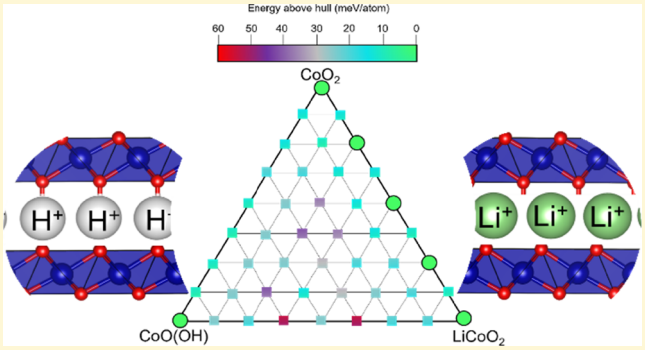

1. INTRODUCTION

As recognized by the 2019 Nobel Prize in Chemistry awarded to John Goodenough, Stanley Whittingham, and Akira Yoshino, Li-ion batteries (LIBs) are of great importance for our society. This very mature technology has become the prime energy storage in portable electronics powering our laptops and cell phones.[1] LIBs are also considered the solution of choice for moving the automotive sector toward electrification and a key enabler to boosting the transition from fossil fuels to renewable energy sources.[2]

Current commercial LIBs are composed of an anode based on carbon and a transition metal oxide cathode separated by an organic liquid electrolyte containing a lithium salt such as $LiPF_6$. The organic electrolyte is flammable, is expensive, and needs to be kept away from any water contamination.[3−6] Therefore, working with an aqueous electrolyte would be extremely beneficial, especially to lower the production cost and achieve higher safety and lower toxicity.

Such aqueous Li-ion batteries (ALIBs) were demonstrated in the foundational work by Li et al., who combined an anode of VO_2 and a cathode of $LiMn_2O_4$ in an aqueous electrolyte.[7] In addition to the obvious lower energy density due to a more restricted voltage electrochemical window, additional fundamental limitations of ALIBs have been identified, such as proton co-insertion.[8−10] Proton insertion has been one of the common rationales for performance issues in ALIBs, such as capacity fading and the increase in Li^+ diffusion barriers.[11,12]

Layered $LiCoO_2$ (LCO) and related compounds are the most widely adopted cathode materials when using organic electrolytes. Indeed, they show a fast charge−discharge reaction for a

Received: June 1, 2021
Revised: August 14, 2021
Published: August 30, 2021

https://doi.org/10.1021/acs.chemmater.1c01887
Chem. Mater. 2021, 33, 6942−6954

potential ranging from ~3.6 (fully lithiated state) to ~4.2 V vs Li^+/Li (charge state at $Li_{0.5}CoO_2$).[13,14] LCO materials have been significantly studied as a cathode in aqueous electrolytes as well, raising questions on the possibilities and mechanisms for proton insertion/exchange. Several studies have investigated chemical proton exchange in LCO. Fernández-Rodriguez et al. reported the irreversible conversion of layered LCO into cobalt oxyhydroxide (CoO(OH)) and spinel Co_3O_4 when carrying out a low-temperature hydrothermal treatment in acid media.[15] Similar results were obtained in a recent study where the proton/ion-exchange reactions in LCO and $NaCoO_2$ (NCO) in aqueous solutions were evaluated, reporting the full protonation of both materials and highlighting the slower H^+/Li^+ exchange in comparison to the fast H^+/Na^+ exchange.[16] Other studies reported the formation of metastable structures containing H^+ and Li^+ intercalated in LCO after chemical treatment in acidic media at very low Li^+ concentrations.[17,18] Moreover, by comparing several cathode materials, Choi et al.[19] concluded that nonlayered cathode materials (such as orthorhombic $LiMnO_2$, spinel $LiMn_2O_4$, and olivine $LiFePO_4$) are less prone to H^+ intercalation than layered materials such as LCO among others. These results were corroborated by density functional theory (DFT) computations.[20] Based on these studies, LCO and, in general, layered oxide materials should, in principle, not be good cathodes for ALIBs due to their facility to exchange protons. Nevertheless, cyclability experiments in ALIBs reported an excellent performance for LCO. Ruffo et al.[21] explored the Li^+ insertion/extraction using a highly concentrated $LiNO_3$ aqueous solution as the electrolyte, obtaining results consistent with the Li (de)intercalation in organic electrolytes. They detected a small potential difference between redox peaks, indicating the fast kinetics of Li^+ ions during the insertion and extraction, without any phase transition. A similar observation was made by Ramanujapuram et al.,[22] who observed a high capacity and a rather stable performance using different concentrations of Li_2SO_4 and $LiNO_3$. They achieved LCO stability with less than 13% degradation (related to surface deterioration) after 1500 cycles, without the leaching effects observed in chemical and electrochemical experiments. These results clearly raise the following question: why can layered LCO perform so well in an aqueous environment while it is prone to proton intercalation?

Here, we address this question using first-principles calculations and investigate the chemical exchange process between alkali ions (Li^+ and Na^+) and H^+. Computing within DFT the energetics of Na^+, Li^+, H^+, and vacancy in different stackings of layered cobalt oxide, we perform a thermodynamic analysis studying the voltage−composition dependence and thermodynamic phase stability. We compare our results to the experimental knowledge and discuss the role of thermodynamics and kinetics in proton insertion within $LiCoO_2$ and $NaCoO_2$.

2. COMPUTATIONAL DETAILS

2.1. First-Principles Calculations. Periodic DFT calculations were carried out using the Vienna ab initio Simulation Package code.[23] The exchange-correlation energy was modeled through the generalized gradient approximation (GGA) using the Perdew−Burke−Ernzerhof (PBE)[24] functional. The valence electron wavefunctions were expanded onto a plane-wave basis set. The effect of the core electrons is taken into account through the projector augmented wave method of Blöchl[25] as implemented by Kresse and Joubert.[26] The Brillouin zone was sampled by a 5 × 5 × 3 grid of *k*-points within the Monkhorst−Pack scheme.[27] The atomic positions were relaxed until the forces were smaller than 0.01 eV $Å^{-1}$. At each relaxation step, the self-consistency loops on the electronic density were stopped when the energy difference was less than 10^{-4} eV from one iteration to another. The DFT + *U* formalism was used following the method suggested by Dudarev and Botton[28] to describe better the local character of the strongly correlated 3d electrons of the Co atoms. We chose a U_{eff} value of 3.2 eV as suggested by the Materials Project database[29] to describe $LiCoO_2$ and $NaCoO_2$ materials.

2.2. Structure and Computational Models. Figure 1 shows the $ACoO_2$ layered compounds investigated in this work.

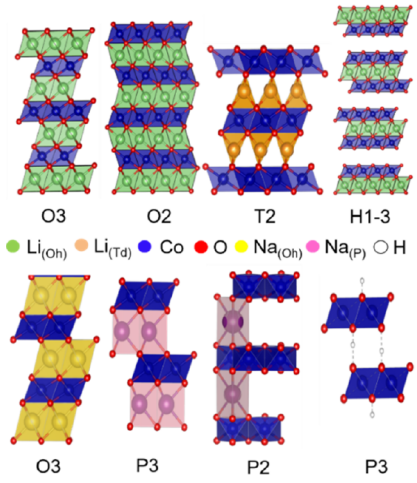

Figure 1. Polyhedral and ball-and-stick representation of the different layered structures of Li_xCoO_2, Na_xCoO_2, and CoO(OH). The Co atoms inside CoO_6 octahedra are depicted in blue. The Li atoms inside either LiO_6 octahedra (O3, O2, and H1-3) or LiO_4 tetrahedra (T2) are indicated in green and orange, respectively. The Na atoms inside either NaO_6 octahedra (O3) or NaO_6 prisms (P2 and P3) are sketched in pink and yellow, respectively. The H atoms are shown in white.

They all present a structure with close-packed oxygen layers alternating with either A cations (H, Li, and Na in this study) or transition-metal atom (Co) layers. These layered structures can be labeled adopting the notation introduced by Delmas et al.[30] in which the coordination of the site occupied by the "A" cation (O, T, or P for octahedral, tetrahedral, or prismatic, respectively) is followed by the number of different layers repeated in the structure of the material. The most stable LCO is the O3 structure (ABC stacking) with the space group $R\bar{3}m$. Li^+ and Co^{3+} occupy the 3a and 3b Wyckoff positions, respectively.[30] The LiO_6 and CoO_6 octahedra only share edges. The half de-intercalated compound $Li_{0.5}CoO_2$ evolves into a monoclinic structure.[31,32] The latter is thermodynamically unstable, and, for this reason, LCO only delivers half of its theoretical capacity in commercial LIBs. According to different theoretical studies,[33−35] cubic spinel is energetically favored over a layered structure for $Li_{0.5}CoO_2$. In the present work, we have, however, considered that the layered structure is maintained during the H^+ and alkali insertion/extraction process. On the other hand, the O2-$LiCoO_2$ phase (AB stacking) with the space group $P6_3mc$ can also be a suitable candidate cathode in LIBs. The O2 phase is metastable and was prepared for the first time by Delmas et al.[30] In this structure, the LiO_6 octahedra share not only edges but also faces with the CoO_6 octahedra. Other phases such as the tetrahedral (T)—where Li^+ cations are in tetrahedral sites—and

https://doi.org/10.1021/acs.chemmater.1c01887
Chem. Mater. 2021, 33, 6942−6954

the H1-3 phase—a layered phase that alternates O1 and O3 layers, only found at large voltages and very low Li^+ concentrations[32]—have been considered as well. The end member of the delithiation process is CoO_2, a hexagonal simple layered phase called O1.[36,37] For the $NaCoO_2$ layered compounds, the O3 phase is the most stable structure at a full concentration of Na. Nevertheless, it is well known that the two-layer-type phase P2 (ABBA stacking) is stable at different concentrations of Na. In contrast with the O phases, the cations in the P phases form prisms between the CoO_2 layers.[38] The P2-$Na_{0.70}CoO_2$ phase is stable, and it was found to be the precursor of O2-$LiCoO_2$ by Li^+/Na^+ exchange since Li^+ atoms prefer O sites.[39] The P3-$NaCoO_2$ phase ($R\bar{3}m$) has been characterized,[40−42] and it has been considered to explore the H^+/Na^+ exchange. In this stacking, Na atoms are located in P sites following an ABC stacking. Note that both P phases can evolve easily toward the O phases through a lateral stacking displacement. As for the protonated systems, different structures were computed to investigate the H^+ sites in the lattice. The P3-CoO(OH) structure (space group of $R\bar{3}m$) first described by Delaplane et al.[43] and available in the Materials Project database (mp-27913)[29] was selected. The O3-CoO(OH) polymorph was generated by substituting Li^+ (Na^+) by H^+ in O3-$LiCoO_2$ (O3-$NaCoO_2$, respectively). The P2-CoO(OH) configuration with the space group $P6_3/mmc$ was chosen as the reference for P2/O2 structures (available in the Materials Project database, mp-743839).

Our model contains an eight-unit formula of the $ACoO_2$ ($2 \times 2 \times 2$) supercell. The latter contains two O−alkali−O layers, with four available sites on each layer. This is very useful to compare the interaction of alkali, protons, and vacancies because the presence of two layers makes it possible to investigate the preference of alkali/H to be placed in the same layer or in a different layer.

Several binary and ternary orderings combining [Li^+−Vac], [Na^+−Vac], [H^+−Li^+], [H^+−Na^+], [H^+−Li^+−Vac], and [H^+−Na^+−Vac] ions have been considered in both O and P stackings. To discriminate among the different arrangements with the same amount of H^+−Na^+/Li^+−Vac on the host structure, the electrostatic energy of the corresponding periodic array of charges was first calculated using the Ewald summation method[44] implemented in pymatgen.[45] This method calculates the electrostatic energy of a periodic array of charges using the Ewald technique, reproducing results similar to those obtained with the GULP code.[46,47] Thus, the accuracy is sufficient as a first step to discriminate among different arrangements. Then, the total energy was computed using DFT for 10 of the lowest energy structures according to the Ewald sum.

First of all, the binary [Li^+−Vac], [Na^+−Vac], [H^+−Li^+], and [H^+−Na^+] systems were investigated in O and P stackings, starting from DFT-optimized fully protonated and fully lithiated/sodiated systems. The H^+/alkali exchange was investigated displacing the ions toward their most favorable sites (whenever necessary) according to preliminary stability analysis. In order to obtain the candidate structures for [H^+−Li^+−Vac] and [H^+−Na^+−Vac], the same approach has been followed. To ensure that important arrangements were not missed, additional structures with 50% or more of Na^+ or Li^+ concentration were also generated. It is important to investigate exhaustively these configurations since the typical voltage applied in battery experiments ensures the presence of at least 50% of Li^+ and Na^+ in the host structure. To generate this additional set of structures, the binary arrangements [H^+−Na^+] and [H^+−Li] with the lowest DFT energy and more than 50% of alkali concentration were selected. Then, the H^+ ions were systematically removed, and these configurations were reoptimized by means of DFT.

2.3. Voltage. The equilibrium $H^+/Li^+/Na^+$ intercalation voltage was calculated as the difference in the cation chemical potential between the cathode and the anode. The chemical potential is directly related to the Li^+/Na^+ intercalated voltage:

$$V = -\frac{\mu_A^{\text{cathode}} - \mu_A^{\text{anode}}}{zF} = -\frac{\mu_A - \mu_A^{\text{ref}}}{zF} \quad (1)$$

where z is the transferred charge, F is the Faraday constant, and A may represent H^+, Li^+, and Na^+ in this work. The chemical potential reference for metallic Li and Na (body-centered cubic) was also obtained from first-principles calculations (−1.91 and −1.31 eV, respectively). The cell voltage is also related to the H chemical potential, μ_H^{ref}, obtained as the DFT energy of 1/2 H_2, following the computational hydrogen electrode model proposed by Nørskov et al.[48] Following eq 2, the average intercalation voltage was estimated using DFT for fully charged and discharged cathodes (e.g., $NaCoO_2$ and CoO_2). To compute the complete voltage curve, the stability of the phases with intermediate $H^+/Li^+/Na^+$ concentrations must be explored. Thus, the formation energy of these intermediate phases was calculated by reference to the fully charged and discharged phases

$$E_f = E[A_xCoO_2] - x\,E[ACoO_2] - (1 - x)\,E[CoO_2] \quad (2)$$

The convex hull was determined with all of the thermodynamically stable phases compared with the reference phases, plotting their formation energy as a function of the composition. Then, a voltage profile could be obtained through eq 1 applied to adjacent phases. Combining the convex hull with the voltage curve, it was possible to determine the phase-transition voltage (cation insertion/extraction).

2.4. Phase Diagram and Grand Potential Phase Diagram. The ground-state ternary phase diagram was obtained by analyzing the stability, thanks to the convex hull for the intermediate phases containing H^+, Li^+, Na^+, and vacancies for the fully charged ($ACoO_2$), fully protonated (CoO(OH)), and fully discharged phases (CoO_2). The simulated 0 K phase diagrams compare quite well with the experimental ones at finite temperatures, as already discussed in previous works.[33,49−52] Approaches such as the cluster expansion can be used to include temperature effects, but this comes to a much higher computational price for differences between 0 K and finite temperature phase diagrams that are subtle.[52] Typically, some of the configurations with small energies above hull might become stable at finite temperatures. Usually, constructing the 0 K phase diagrams is thus sufficient to gain qualitative insight to estimate the phase stability because they are expected to reproduce fairly well the experimental phase diagrams at finite temperatures.

In an electrochemical device, a grand canonical approach is more appropriate with a system open to the moving species (Li^+, Na^+, or H^+).[49,53] The thermodynamic potential of each phase in these conditions can be written as the Legendre transform of the Gibbs free energy as follows:

$$\gamma = G - n_H \times \mu_H - n_A \times \mu_A \quad (3)$$

https://doi.org/10.1021/acs.chemmater.1c01887
Chem. Mater. 2021, 33, 6942−6954

where G is the free energy approximated by the DFT energy for a particular ordering (at low temperatures, the entropic contribution can be neglected), n_H and n_A are the amounts of hydrogen and cation A in the material, respectively, and μ_H and μ_A are the chemical potentials of H^+ and the A cations, respectively. The more negative the γ, the higher the stability of the system. One can explore the phase stability in any particular H^+, Li^+, and Na^+ chemical potential, which can be directly related to the battery voltage

$$\mu_H^{ref} - \mu_H = V \text{ vs } (H^+/H_2) \quad (4)$$

$$\mu_{Li}^{ref} - \mu_{Li} = V \text{ vs } (Li^+/Li) \quad (5)$$

$$\mu_{Na}^{ref} - \mu_{Na} = V \text{ vs } (Na^+/Na) \quad (6)$$

where V is the battery voltage with respect to the H^+, Li^+, and Na^+ reduction potential for 1e$^-$ transfer and the chemical potential expressed in eV. Moreover, the voltages with respect to H^+, Li^+, and Na^+ reduction are linked,

$$E^0[H^+/H_2] = 0.00 \text{ V vs } E^0[H^+/H_2] \quad (7)$$

$$E^0[Li^+/Li] = -3.045 \text{ V vs } E^0[H^+/H_2] \quad (8)$$

$$E^0[Na^+/Na] = -2.714 \text{ V vs } E^0[H^+/H_2] \quad (9)$$

Consequently, the chemical potential (and voltage) of H^+ can be expressed as a function of the chemical potential of Li^+ and Na^+ and vice versa, i.e., for a particular working voltage, these chemical potentials are related as follows:

$$\mu_H^{ref} - \mu_H = V \text{ vs } (Li^+/Li) - 3.045 \text{ V} \quad (10)$$

$$\mu_H^{ref} - \mu_H = V \text{ vs } (Na^+/Na) - 2.714 \text{ V} \quad (11)$$

The amount of Co and O is fixed since we are simulating an insertion battery, where the layered structure is fixed (the stacking can change). Thus, no metal dissolution or oxygen loss is considered. In addition, we considered the effect of the pH and the alkali concentration in the aqueous media to predict the stable phases under experimental conditions through the Nernst equation. Following the definition of pH in eq 10, the μ_H changes and it affects the phase stability (γ). The same effect occurs including the alkali concentration

$$pH = -\frac{\ln a_{H^+}}{\ln 10} \quad (12)$$

$$\mu_H = \mu_H^{ref} + k_B T \ln a_{H^+} \quad (13)$$

$$\mu_H = \mu_H^{ref} - k_B T \ln 10 pH \quad (14)$$

$$\mu_A = \mu_A^{ref} + k_B T \ln a_A \quad (15)$$

$$\mu_A = \mu_A^{ref} + k_B T \ln[A^+] \quad (16)$$

where k_B is the Boltzmann constant, T is the temperature under standard conditions, and a is the activity of the species that is supposed to be ideal.

3. RESULTS

3.1. Results of LCO. *3.1.1. Stability of LCO and H-Intercalated Structures.* The LCO structures reported in Figure 1 were taken as the starting structure to model the LCO structures with vacancies ($Li_{1-x}CoO_2$). Several orderings and arrangements containing Li^+ and vacancies have been generated, simulating a delithiation (charging) process.

Experimentally, the O3 structure is found to be the most stable phase in the fully lithiated state. However, the stacking of the structures can be modified during the alkali insertion/extraction process.[31,39] Figure 2 shows the formation energy of

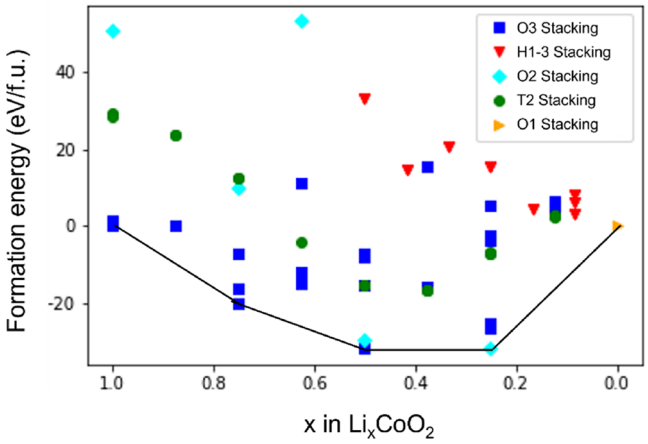

Figure 2. Convex hull of the different ordered Li_xCoO_2 structures as a function of the Li^+ concentration as computed by PBE + U.

$Li_{1-x}CoO_2$ as a function of the Li^+ content. The convex hull shows that the O3 structure is the most favorable phase for Li^+ contents ranging from 100% to 25%. It may be possible to find stable phases under different Li^+ concentrations values considered in our model, although the obtained results are in agreement with previous theoretical simulations as well as experimental studies using organic electrolytes.[54,55] At 25% content of Li^+, the calculations predict that O2 stacking becomes the most energetically stable one by less than 5 meV/atom with respect to O3. In agreement with previous computational and experimental results, our simulations evidence that solid solution (Li^+ vacancy) is energetically favored.

For hydrogenated structures, the convex hull includes two-layered phases differing by their stacking: the experimentally reported P3-CoO(OH) structure and O3 structure obtained from exchanging H^+ with Li^+ in O3-$LiCoO_2$. In the latter, H^+ ions were placed at the center of the octahedra and slightly displaced toward the O atoms. After relaxation, some configurations stayed as O3, but the H^+ ions were displaced toward one of the O atoms tending to form an −OH bond (see Figure 3a). Nevertheless, other structures evolve toward P3 stacking. Note that the difference between both structures is the lateral stacking shift of O−Co−O layers. In the P3-type stacking, H^+ ions are accommodated between the O layers, forming interlayer hydrogen bonds (O−H−O), as is depicted in Figure 3b. The formation of OH moieties is in agreement with other computational studies[11] and the experimental literature.[56,57] The convex hull of dehydrogenation of CoO(OH) is shown in Figure 3c. The P3 structures are significantly more stable than the O3 structures. The greater stability of P3 can be attributed to the absence of hydrogen bonds in the O3 structures. None of the partially protonated $CoO(OH_{1-x})$ structures are lower in energy than the linear combination of CoO(OH) and CoO_2. In contrast with LCO, the CoO(OH) solid solution is not energetically favored. Co−O−H forms a biphasic system. The geometries with partial hydrogenation are found to be 8−15 meV/atom above hull depending on the H^+ concentration. We

https://doi.org/10.1021/acs.chemmater.1c01887
Chem. Mater. 2021, 33, 6942−6954

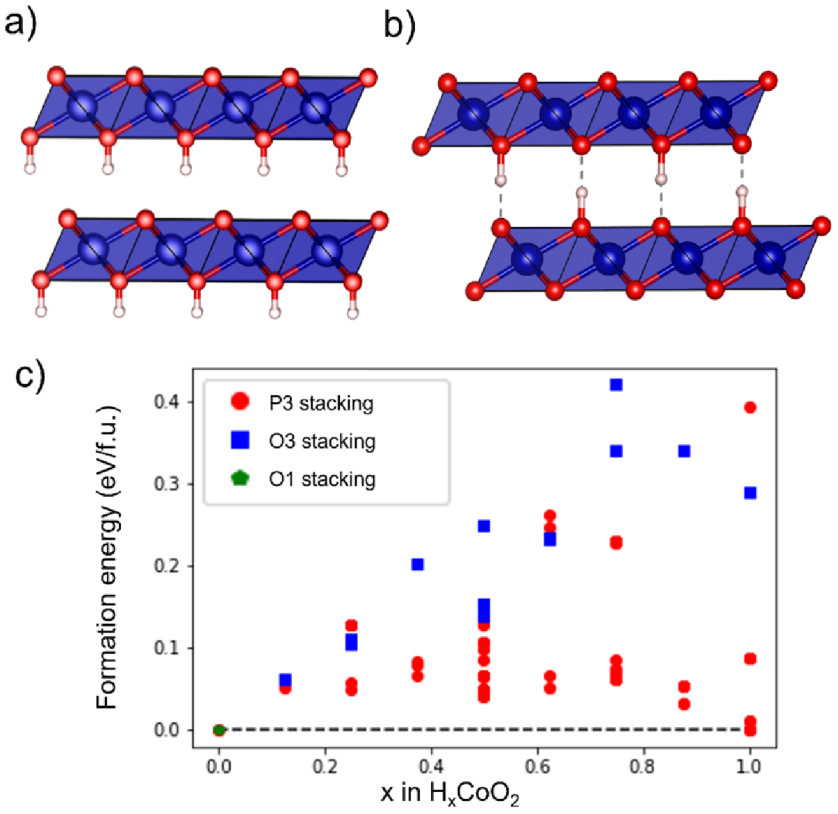

Figure 3. Polyhedral and ball-and-stick representation of (a) O3-CoO(OH) and (b) P3-CoO(OH). (c) Formation energies of ordered CoO(OH) structures as a function of the H^+ concentration computed by PBE + *U*. The same atom coloring scheme is used as in Figure 1.

suggest that this is due to the large stability of the interlayer hydrogen bonds, which energetically disadvantage the partial protonated structures with respect to the fully protonated compound.

3.1.2. Stability of $Li_xH_yCoO_2$. $Li_{1-x}CoO_2$ and $CoO(OH_{1-x})$ favor very different stackings of the layers (O3 vs P3). The remaining questions are whether it is thermodynamically favorable to have the coexistence of H^+ and Li^+ in the host lattice and which stacking prevails depending on H^+/Li^+ concentrations.

In the present study, CoO_2, O3-$LiCoO_2$, and P3-CoO(OH) are considered as our reference compositions. To find the ground-state cation arrangement, we calculated the energies of several H^+, Li^+, and vacancy cationic configurations, considering possible stacking transitions. Different H^+/Li^+/vacancy orderings were generated starting from the O3, O2, and P3 structures owing to the different stacking preferences of H^+ and Li^+. The O-stacking favors lithium in CoO_2. Note that the P-type phase of the $LiCoO_2$ polymorph is not experimentally stable since Li^+ cannot be stabilized in the large prismatic sites.[39] Nevertheless, we have generated orderings with Li^+ and H^+ in both O and P stackings.

Figure 4 illustrates the ground-state ternary phase diagram of the $LiCoO_2$–CoO_2–CoO(OH) system determined from DFT at 0 K. This phase diagram is shown as an equilateral triangle where the three vertices represent 100% Li^+ (O3-$LiCoO_2$ composition), 100% vacancy (CoO_2 composition), and 100% H^+ (P3-CoO(OH) composition), the most energetically favorable structures for each reference. It is important to note that Li^+ placed initially on P sites moves toward O sites after atomic relaxation. Three delithiated structures—$Li_{0.75}CoO_2$, $Li_{0.5}CoO_2$, and $Li_{0.25}CoO_2$—are predicted to be stable with

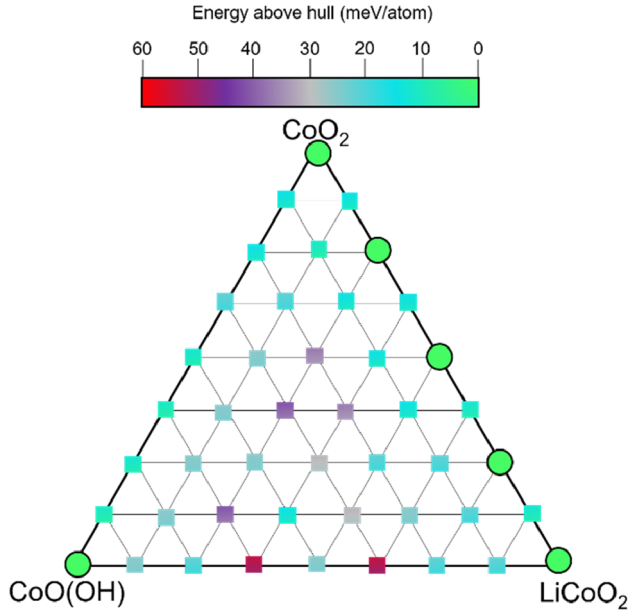

Figure 4. Phase diagram (0 K) of $H_yLi_xCoO_2$ ($x + y \leq 1$) structures computed by PBE + *U* using fully lithiated, fully protonated CoO_2 lattice. Circles indicate the stable compositions, while squares represent structures with energies above hull.

respect to our references in the vertex. This is in agreement with the solid-solution reaction to (de)lithiate the LCO cathode material. On the other hand, our simulations do not predict any stable structure with Li^+ and H^+ coexisting in the CoO_2 lattice. The closest structures containing both ions have energies around 15–19 meV/atom above hull. These orderings have low

https://doi.org/10.1021/acs.chemmater.1c01887
Chem. Mater. 2021, 33, 6942–6954

Li^+ concentration (50% or less) and a very low concentration of H^+ (12.5%). This corresponds to the top-right region of the phase diagram. Since the voltage window applied during battery operations limits the delithiation process, the focus should only be on the compositions with more than 50% of the Li^+ content (bottom-right). In that part of the diagram, all of the generated structures were found to be less favorable compared to the references, with energies more than 20 meV/atom above hull. With respect to the H^+-rich and vacancy-poor portion of the phase diagram (bottom-left), one can observe that these orderings present the largest energies above hull, especially compounds without vacancies. All these results can be explained in terms of stacking competition, structure distortion, and H^+/alkali repulsion, as illustrated in Figure 5, which provides a

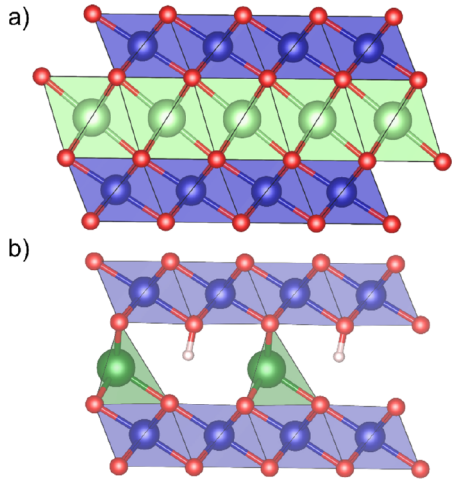

Figure 5. (a) Co−Li−Co layers of O3-$LiCoO_2$ and (b) Co−Li/H−Co layers of $Li_{0.75}H_{0.125}CoO_2$ with partial stacking displacement. The same atom coloring scheme is used as in Figure 1.

comparison between the fully lithiated (Figure 5a) CoO_2 layer and the one with both ions (Figure 5b). The presence of intercalated H^+ induces a significant layer shift, but the phase transition O3 → P3 is not complete. Moreover, a significant distortion of the octahedral site of Li^+ is observed due to the displacement of Li^+ away from the center of the octahedral site. The stacking competition and the subsequent structural distortions imply an energy loss compared to the reference endpoints in the diagram. For this reason, structures that contain low concentrations of both ions (i.e., a large concentration of vacancies) are slightly more energetically favorable than structures with low vacancy concentrations. The presence of vacancies reduces H^+/Li^+ repulsion.

3.1.3. Grand Potential Phase Diagram of H−Li−Co−O. The grand potential phase diagrams have been constructed considering the quaternary $Li_xH_yCoO_2$ ($x + y \leq 1$) structures. In the open H−Li−Co−O system, the stable phases can also be obtained for specific conditions. To describe the cathode stability in battery operations, a grand canonical approach is more appropriate with a system open to the intercalated species. To simulate the battery operation conditions, the chemical potentials of Li^+ and H^+ are related to the applied voltage. As a function of the latter, the μ_{Li} and μ_H increase and decrease and the phase stability may change. Figures 6 and S1 show the grand potential phase diagrams as a function of μ_{Li} and μ_H Along both the x and y axes, the chemical potential values are indicated with respect to their references. The solid red line represents the

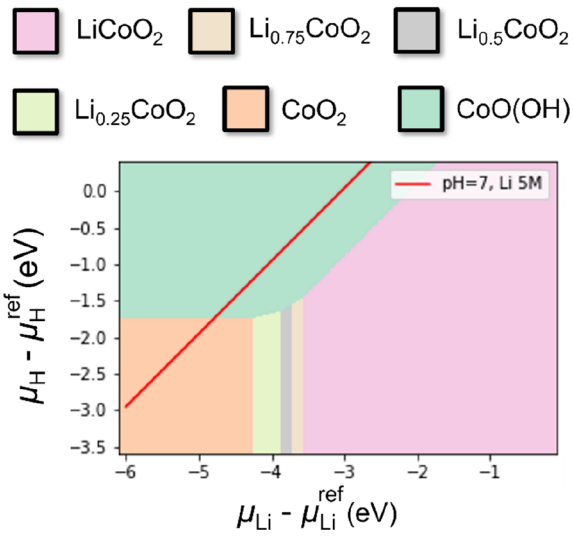

Figure 6. Stable phase of $(H,Li)_xCoO_2$ as a function of the Li^+ and H^+ chemical potentials at pH = 7 and 1 M Li^+. The red line represents the voltage of the reduction potential relation between Li^+/Li and H^+/H_2, simulating the experimental voltage conditions.

physical meaning region where μ_{Li} and μ_H lead to the same voltage equation (eq 8). The computed grand canonical phase diagram reveals the large stability of CoO(OH) independently of the pH conditions at voltages typically applied during battery operations (3.5−4.5 V vs Li^+/Li). From the thermodynamical point of view, the predicted (electro)chemical H^+ insertion proceeds via a first-order phase transition CoO(OH) ↔ CoO_2 at voltages between 4.3 and 5.1 V vs Li^+/Li depending on the pH and the Li^+ concentration (see Figure S1). As the pH is lowered, the stability of CoO(OH) increases with respect to Li^+/vacancy solid solution, and consequently, higher voltages are needed to (de)intercalate H^+ from the host structure (5.1 V at pH = 0, 4.7 V at pH = 7, and 4.3 at pH = 14).

Nevertheless, according to cyclability experiments in aqueous and nonaqueous electrolytes, the reaction proceeds via solid solution reaction ($LiCoO_2$ ↔ $Li_{0.5}CoO_2$).[21,22] These results clearly evidence that CoO(OH) is the thermodynamic product of the H^+/Li^+ insertion in the CoO_2 lattice, whereas the cyclability process is governed by kinetics, promoting the Li^+ (de)intercalation.

3.1.4. Voltage−Composition Curves. The voltage plots as a function of H^+ and Li^+ concentration (x_H and x_{Li}) in the CoO_2 lattice have been computed to investigate if the H^+ insertion causes changes in the Li^+ (de)intercalation working voltage. The 0 K voltage curve for Li^+ (de)intercalation (Figure 7a) agrees with previous DFT studies[11,58] and the experimental curve in organic electrolytes[59] apart from an underestimation of ∼0.3 V, which is in line with the typical error in voltages using GGA + U.[60] The DFT voltage curve has a few voltage steps, originating from the ground-state orderings at different Li^+ concentrations detected in the convex hull plot (Figure 2). The voltage steps clearly show that the Li^+ (re)insertion process is governed by a solid solution reaction. In contrast, these steps are not observed in the (de)hydrogenation voltage curve, which is clearly flat, displaying a two-phase behavior at a working voltage significantly higher than Li^+ (de)intercalation.

Our computations predict the voltage of H^+ cyclability between CoO_2 and CoO(OH) to be beyond 5 V vs Li^+/Li. Using our grand canonical potential result (Figure 6), we expect

https://doi.org/10.1021/acs.chemmater.1c01887
Chem. Mater. 2021, 33, 6942−6954

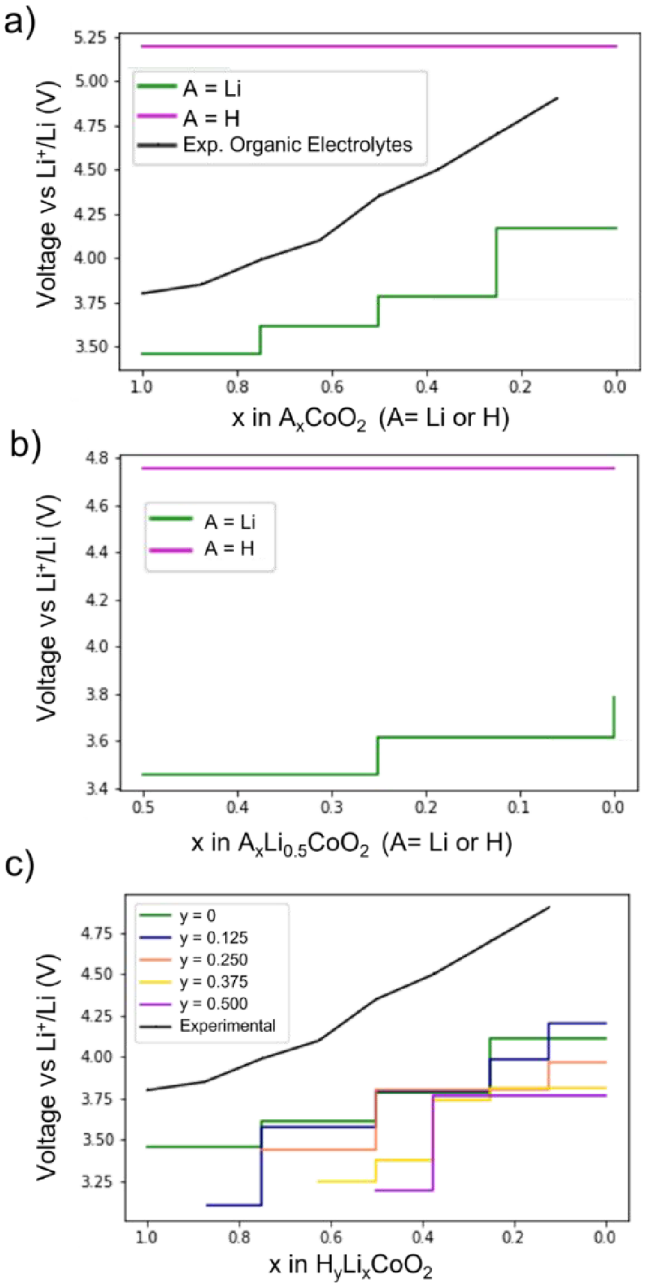

Figure 7. (a) Voltage−composition plot of Li^+ (green) and H^+ (pink) insertion/extraction process. Experimental voltage of $LiCoO_2$ is depicted by the solid black line. (b) Voltage−composition plot of the Li^+ (green) and H^+ (pink) insertion/extraction process using $Li_{0.5}CoO_2$ as the end member. (c) Voltage plot of Li^+ insertion/extraction assuming a constant concentration (y) of H^+. Solid green, blue, orange, yellow, and purple lines show working voltages at 0%, 12.5%, 25%, 37.5%, and 50% of H^+ concentration in the host structure.

that a $LiCoO_2$ cathode in an aqueous electrolyte will thermodynamically favor its full protonation forming CoO(OH). If this process was indeed happening in ALIBs, the operating voltage for obtaining current and deintercalated protons would be much higher (and probably not achievable without electrolyte decomposition). Indeed, Figure 7b shows the comparison between Li^+ and H^+ intercalation processes at partially lithiated LCO. Using $Li_{0.5}CoO_2$ as the end member, the discharged structure with the lowest Li^+ concentration according to experiments, we have predicted the intercalation voltage of Li^+ and H^+. The voltage to mix Li^+ and H^+ in the same lattice is more than 1 V higher than the solid-solution reaction between $Li_{0.5}CoO_2$ and $LiCoO_2$. The mixed H^+/Li^+ voltage curve from $Li_{0.5}CoO_2$ to $H_{0.5}Li_{0.5}CoO_2$ is clearly flat and is described as a two-phase transition at voltages beyond 4.6 V. In contrast, $Li_{0.5}CoO_2$ takes up Li^+ in a solid-solution reaction up to about $LiCoO_2$ at voltages applied during battery operations. We hypothesize that the difficulty in mixing H^+ and Li^+ in the same structure (due to their very different stacking preferences) requires the nucleation of large fully protonated regions, a process that is likely to be difficult kinetically. It can justify the slow H^+/Li^+ detected in hydrothermal experiments.[16]

Although cyclability experiments are governed by kinetics (showing the LCO (de)lithiation process) and the voltage required to (de)intercalate H^+ is predicted to be much higher than the experimental working voltage, the chance of H^+ insertion is not fully ruled out and to know their possible effect in battery performance is a must. Figure 7c illustrates the influence of H^+ intercalation on the working voltage. The voltage−composition curve has been plotted considering partial H^+/Li^+ exchange. The voltage of Li^+ insertion/extraction has been computed at different H^+ concentrations, i.e., these structures contain some intercalated H^+ instead of Li^+ atoms. As shown in Figure 7c, the presence of protons in the host structure slightly lowers the working voltage (0.1−0.2 V) of structures that host H^+ with respect to the voltage curve without H^+. In other words, hosting H^+ comes with an energy loss that increases the number of H^+ that are in the layered lattice. The energy loss is related to the small distortions generated by the repulsion of Li^+ and H^+ in the same layer and the different stacking preferences. Our results suggest that the H^+ insertion could be detected because the redox peaks would be slightly shifted toward lower voltages compared to the solid solution. However, the experiments using LCO as the cathode material in aqueous electrolytes were consistent with those expected for the insertion and extraction of lithium, without a shift in the redox peaks, which seems to discard a noticeable H^+ intercalation.[21]

3.2. Results of NCO. *3.2.1. Phase Diagram.* The above results indicate that the stacking competition of H^+ and Li^+ is central to the thermodynamics and kinetics of proton and Li^+ insertion in layered cobalt oxide. Sodium cobalt oxide is also a cathode material of interest and presents notably very different stacking preferences. Different stackings (O3, P3, and P2) are typically observed during the Na^+ charge/discharge process.[30,50,61] NCO can thus be considered a good reference for an in-depth study of the role of the ion nature and the stacking in H^+ insertion. As it occurs with LCO, only half of the theoretical capacity of NCO can be reached, although in this case, it is because the stacking transition from O3 to P3 occurs when the Na^+ content is lower than 0.5.[62] To ascertain if H^+ can intercalate in NCO, we assessed the phase stability of P2 and O3/P3 systems, exploring different concentrations of Na^+, H^+, and vacancies following the same procedure carried out in the LCO section.

The end member O3-$NaCoO_2$ is slightly lower in energy than P2 and P3-$NaCoO_2$.[63,64] Nevertheless, to compute the P2-type phase diagram, only P2-type structures were considered since the P2−P3 phase transition does not occur during Na^+ cyclability.[65] As illustrated in Figure 8, one structure containing an equimolar concentration of Na^+ and H^+ was predicted to be stable. The simultaneous presence of both species in the P2-type structure agrees with H^+ insertion experiments for the P2-Na_xCoO_2 material.[16] The structures with higher energy above

https://doi.org/10.1021/acs.chemmater.1c01887
Chem. Mater. 2021, 33, 6942−6954

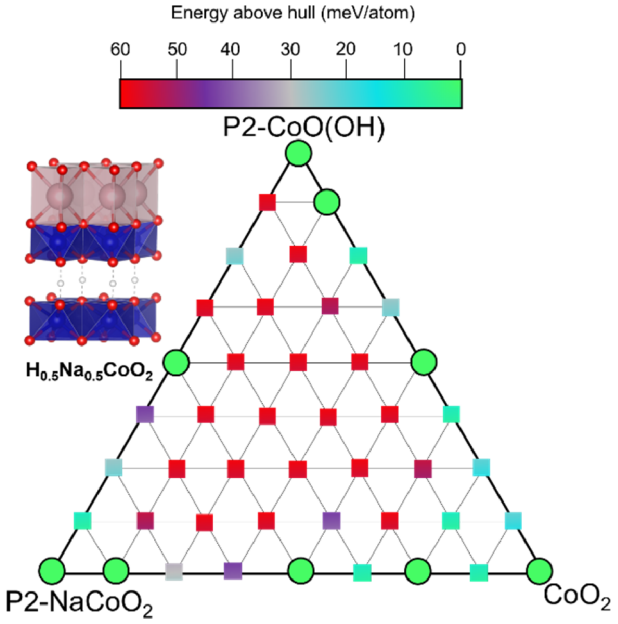

Figure 8. Phase diagram (0 K) of the P2-type structure of $(H,Na,)_xCoO_2$ computed by PBE + *U*. Green circles indicate the stable compositions. The polyhedral and ball-and-stick representation of the stable P2-type $Na_{0.5}H_{0.5}CoO_2$ is also depicted. Red squares show structures with an energy above hull greater than 60 meV/atom.

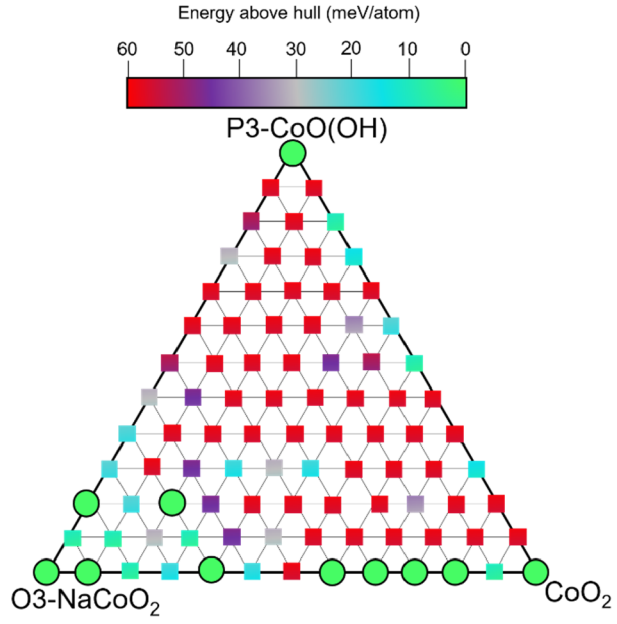

Figure 9. Phase diagram (0 K) of O3- and P3-type structures of $(H,Na)_xCoO_2$ computed by PBE + *U*. Green circles indicate the stable compositions, while the squares represent configurations with energies above hull. Red squares show structures with an energy above hull greater than 60 meV/atom.

hull are located in the central region of the phase diagram, where the concentration of vacancies, Na^+, and H^+ is similar. On the other hand, two orderings that contain both ions were found to be less than 9 meV/atom above the convex hull (cyan squares). Both are located on the H^+-poor portion of the phase diagram (bottom). One of them has high Na^+ concentration ($H_{0.125}Na_{0.875}CoO_2$, bottom-left) and the other one has low concentration of both ions ($H_{0.125}Na_{0.125}CoO_2$, bottom-right). Several structures hosting only Na^+ or H^+ were also found to be stable, showing the stable solid solutions between CoO_2, $NaCoO_2$,[61,65] and CoO(OH). As expected, the prismatic stacking P2 can accommodate intercalated H^+ due to the oxygen alignment between layers. Furthermore, the alternated H^+/Na^+ layers favor the structure stability, avoiding possible energy loss related to H^+/Na^+ repulsion.

Figure 9 illustrates the simulated DFT (0 K) phase diagram using O3/P3 $NaCoO_2$ and P3-CoO(OH) as end members. In agreement with previous computational studies,[66] the homogeneous solid-solution reaction between Na^+ (re)insertion compounds is energetically favorable, since a few Na^+/vacancy orderings were found to be stable[65] (bottom region). Aside from these structures, only the Na^+-rich zone of the phase diagram shows stable compounds; two structures containing Na^+ and H^+ simultaneously are showing up (green circles). Besides, a few structures with Na^+ and intercalated H^+ have energies lower than 10 meV/atom. These structures present two different kinds of stacking distribution. Figure 10 depicts four of those structures. Figure 10a,b (stable and 10 meV/atom above hull, respectively) presents an O-stacking, in which H^+ are bonded to O atoms close to the Na^+ vacancies site, without promoting the stacking shift or the distortion of Na^+ sites. On the other hand, the $Na_{0.66}H_{0.17}CoO_2$ structure depicted in Figure 10c (stable) and the $Na_{0.83}H_{0.08}CoO_2$ structure (Figure 10d, 10 meV/above hull) highlight the importance of the ion nature and the stacking regarding H^+ insertion. In these structures, layers containing

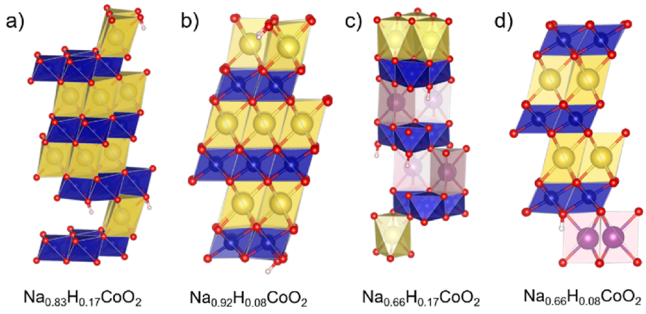

Figure 10. Polyhedral and ball-and-stick representation of different layered structures of O/P-$H_yNa_xCoO_2$ ($x + y \leq 1$). The same atom coloring scheme is used as in Figure 1. (a) $Na_{0.83}H_{0.17}CoO_2$ (stable), (b) $Na_{0.92}H_{0.08}CoO_2$ (10 meV/atom above convex hull), (c) $Na_{0.66}H_{0.17}CoO_2$ (stable), and (d) $Na_{0.66}H_{0.08}CoO_2$ (10 meV/atom above convex hull).

only Na^+ maintain the O-stacking, whereas Na^+ atoms are displaced to P sites when H^+ ions are inserted in the same layer. As a result, an O/P stacking combination is obtained. In previous works, the O/P stacking combination containing only Na^+ was not predicted to be stable compared to the O3 and P3 stackings of Na_xCoO_2.[60] Nevertheless, Kim et al. recently discovered an O/P stacking combination at a high charge state for O3-$NaTi_{0.25}Fe_{0.25}Co_{0.25}Ni_{0.25}O_2$ as the cathode material.[67] Furthermore, Balsys and Davis reported a combined [Li,Na]-CoO_2 intergrowth structure ordered with alternating Li^+ (O sites) and Na^+ (P sites).[68] These O/P structures containing [Na^+,Na^+],[67] [Li^+,Na^+],[68] and [Na^+,Na^+/H^+] (this work) are stable due to the versatility of Na^+ to be placed in both O and P sites.

Finally, the grand potential phase diagram has been constructed considering the quaternary $Na_xH_yCoO_2$ ($x + y \leq 1$) structures, following the same methodology applied for LCO configurations. We have differentiated between P3/O3 (Figure

https://doi.org/10.1021/acs.chemmater.1c01887
Chem. Mater. 2021, 33, 6942−6954

S2) and P2/O2 configurations (Figure S3). As observed in Figures S2 and S3, the protonated polymorphs are the most favorable configurations at battery operation conditions, as already observed for lithiated configurations in previous experimental studies. The P2/O2 configurations are higher in energy with respect to P3/O3 structures, and some partially protonated polymorphs are predicted as stable.

In summary, it is evidenced that the protonated polymorphs are the lowest energy configurations independent of whether the cathode material contains Na^+ or Li^+ in the structure. According to our computations, the difference between LCO and NCO cathode materials is that the latter can accommodate H^+ and Na^+ simultaneously in the host structure, which can accelerate the H^+ by Na^+ exchange, as observed in experiments.[16]

3.2.2. Voltage−Composition Curves. The voltage plots as a function of H^+ and Na^+ concentration (x_H and x_{Na}) have been computed. Figure 11a shows the voltage−composition diagram for the different O and P stackings considered in this work, including the P2-type experimental voltage−composition[62] plot in organic solvent electrolytes. In general, an underestimation of ∼0.3 V related to DFT errors is observed. As expected, the solid solution of CoO_2 and $NaCoO_2$ is formed for both P2 and O3/P3 stackings. Concerning the H^+ (de)intercalation, the O3/P3 system shows the same two-phase solution between CoO_2 and CoO(OH) obtained for the LCO voltage plot in Figure 7, since we have used the same CoO_2 and CoO(OH) geometries as end members. Nevertheless, P2 stacking stabilizes the solid solution phase of H^+/vacancies on P2-type stacking. To simulate this voltage composition curve, only the P2-type structures have been considered, despite P3-CoO(OH) being energetically favorable than P2-CoO(OH). As concluded for LCO, the required voltages to promote H^+ insertion and intercalation are higher than the voltage commonly applied in ASIBs (2.31−3.53 V vs Na/Na^+) due to the H_2 and O_2 evolution reactions.[69]

As observed for LCO, the operating voltage to intercalate the protons is higher than the voltages needed to cycle Na^+. It demonstrated the tendency of the CoO_2 lattice to host H^+ instead of alkali elements either in P or O stackings. However, these results present a remarkable difference with respect to LCO:H^+ insertion is not kinetically hindered. The H^+/Na^+ coexistence in the same layer is predicted to be stable, and therefore, there is no stacking competition, as is suggested for the LCO cathode material. Thus, we hypothesize that H^+ may be inserted on Na_xCoO_2 during battery operations. Figure 11b,c shows the effect of H^+/Na^+ exchange on working voltage during the sodium extraction/insertion process. In total, 25% and 50% of the Na^+ content have been replaced by H^+ to evaluate the effect of H^+ insertion. In general, the same tendency observed for the LCO material is observed for the NCO material, where the voltage slightly decays as the concentration of H^+ in the lattice increases for both stacking phases. However, at 25% of H^+ concentration, a few ground states that host protons show a very slight increase in the working voltage, showing the stability of P-type stacking to accommodate protons compared to octahedral LCO.

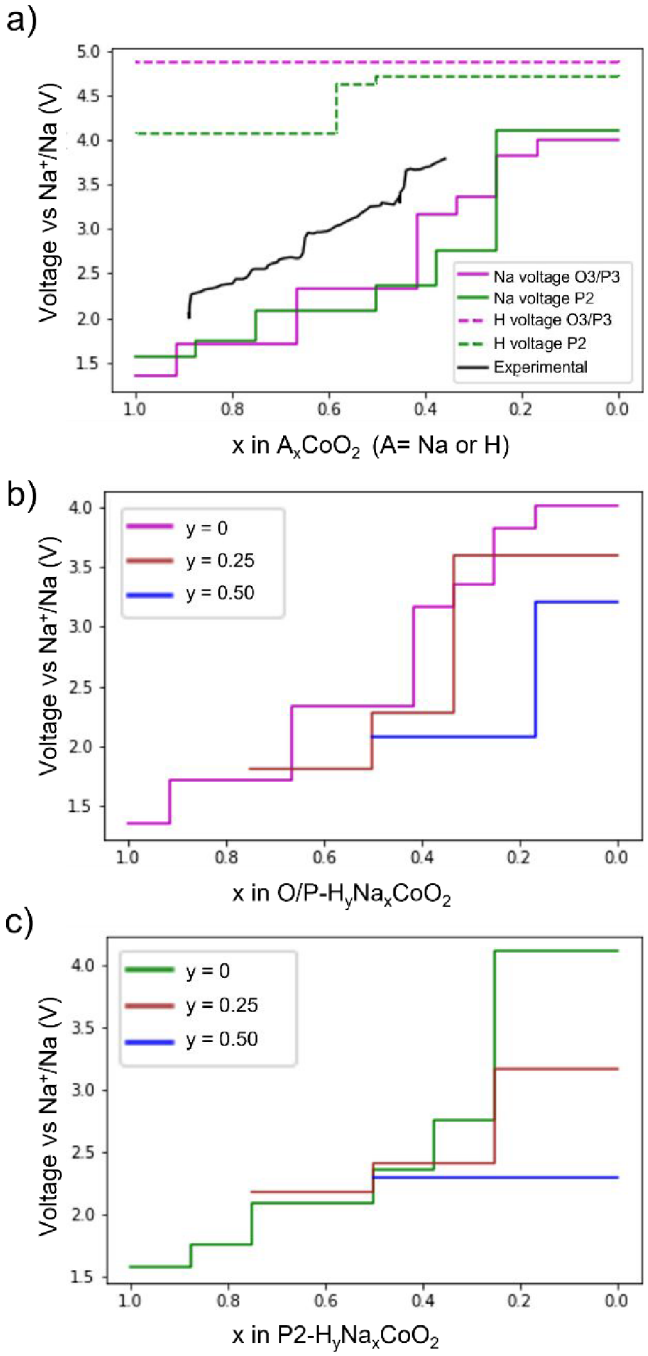

Figure 11. (a) Voltage−composition plot for Na^+ (solid lines) and H^+ (dashed lines) insertion/extraction for O/P3-type (pink) and P2-type (green). Experimental voltage of P2-type Na_xCoO_2 is depicted by the solid black line. Voltage−composition plot of Na^+ insertion/extraction for (b) O3/P3-type and (c) P2-type host structures, assuming a constant concentration (y) of H^+. Solid brown and solid blue lines show the working voltages at 25% and 50% of H^+ concentration.

4. DISCUSSION

In this work, we have calculated the phase stability and the voltage−composition curves for the Li^+ and Na^+ analogues of $ACoO_2$ layered cathode materials using first-principles calculations. We have investigated the possible intercalation of H^+ during the insertion/extraction process and its effect on voltage, phase stability, and battery performance in comparison to experimental knowledge. We have found that the different stacking phases in these materials significantly depend on H^+ intercalation in the host structures.

4.1. CoO(OH) Stability. The greater stability of CoO(OH) compared to $LiCoO_2$ and $NaCoO_2$ may be explained through the formation of interlayer hydrogen bonds. The calculated voltage−composition curves (Figures 7 and 11) show a higher voltage for H^+ than for the alkali insertion/extraction, highlighting that the CoO_2 lattice prefers to host H^+. We

https://doi.org/10.1021/acs.chemmater.1c01887
Chem. Mater. 2021, 33, 6942−6954

believe that the significantly higher energy gain for H^+ insertion compared to Li^+ and Na^+ insertion can be related to the tendency to form H−O bonds compared to Li−O and Na−O bonds. The importance of the P-type stacking is related to the O−O alignment between layers, which favors the formation of highly stable hydrogen bonds. In addition, using DFT computations, we have demonstrated the stability of CoO(OH) as a function of the chemical potentials of Li^+ and H^+, simulating the experimental voltage and pH conditions applied in cyclability experiments. The computed grand potential phase diagram agrees with the hydrothermal experiments that prove the full extraction of alkali elements and the irreversible H^+ intercalation.[15,16] Thus, despite the fact that CoO(OH) is not observed during cyclability experiments, there is no doubt that the fully protonated structure is the most stable phase when Li^+ or Na^+ ions are competing with protons.

4.2. Kinetics vs Thermodynamics. Hydrothermal and thermostability experiments, together with our simulated grand canonical potential, reveal that CoO(OH) is the thermodynamic insertion product of LCO and NCO in aqueous media. We expect that the H^+ by Li^+/Na^+ exchange reaction occurs in LCO and NCO cathode materials when they are immersed in aqueous electrolytes. Nevertheless, our simulations proved that the operating voltage to obtain the protonated material and carry out the de(intercalation) of H^+ is much higher (~4.8 V vs Li^+/Li) than the voltage applied during battery operations. This voltage range is not achievable during battery operations because it would imply the full delithiation of the LCO cathode material and the electrolyte decomposition. Owing to the difficulty in mixing protons and lithium in the same structure, one can hypothesize that protonation requires first the full delithiation of LCO and/or the nucleation of large, fully protonated regions—as it is predicted for single $LiFePO_4$ particles during lithiation.[70,71] However, these two processes are likely to be difficult kinetically.[72]

According to hydrothermal experiments, the H^+ for Li^+ exchange is slow even in acidic media, and it takes 48−72 h to observe the conversion. Despite the fact that the full protonated compound is thermodynamically favored, its formation is kinetically hindered. Our computations suggest that mixing H^+ and Li^+ in the same lattice is impeded due to the stacking competition between H^+ and Li^+ and their repulsion, which slows down the H^+/Li^+ exchange. This fact implies that during cyclability operations, the H^+ intercalation is not observed. The experiments at high Li^+ salt concentrations in water show that the cathodic and anodic peak potentials are close. This is related to fast kinetics and hence favors kinetic products (Li^+/vacancy solid solution) rather than thermodynamic ones (CoO(OH)).

Aside from the high voltage needed, other factors favor the formation of solid solution through Li^+ (de)insertion during LCO cyclability instead of the thermodynamic product; during the hydrothermal investigations, the samples are immersed in the acidic solution until complete alkali extraction and the subsequent protonation.[15,16] In addition, these experiments were carried out under acid media conditions in pure water without Li^+ salts. Notwithstanding, the H^+ by Li^+ exchange reaction in the CoO_2 lattice is very slow even under these, a priori, favorable conditions. In contrast, the Li^+ extraction is limited to 50% Li^+ content during the cyclability process due to the voltage applied in battery operations. Moreover, the battery experiments were performed at pH = 7 in "water in salt" electrolytes,[39] i.e., highly concentrated Li^+ salts. In battery operations, the Li^+ concentration in the electrolyte is 6−7 orders of magnitude greater than the H^+ concentration (1×10^{-7} M at pH = 7). The influence of the electrolyte concentration may affect the diffusion coefficients of H^+ and Li^+ in the electrolyte. The conductivity of H^+ decreases in aqueous Li^+ salts compared to pure water, probably related to lower mobility and the possible attraction of H^+ by Li^+ salts anions in the electrolyte.[73]

Thus, using an operational voltage much lower than that required to obtain the protonated lattice, in addition to the battery operation conditions, leads to the kinetically favored solid solution instead of the H^+ by Li^+ exchange reaction during cyclability experiments.

4.3. Importance of Voltage Window, Ion Nature, and Stacking. The insertion of H^+ would lead to the incomplete stacking transition predicted by our computations (O3 → P3) with considered distortions in the Li^+ sites. These distortions, together with the stacking displacement and H^+/Li^+ repulsion, may not be kinetically favorable with respect to the LCO solid solution. Moreover, we have investigated the effect of possible H^+ insertion on Li^+ (de)intercalation voltage. The voltage−composition plots show a decay at around 0.2 V in working voltages after H^+ accommodation. However, this decay is not detected during cyclability experiments, suggesting that H^+ ions are not intercalated in the CoO_2 lattice.

According to our computations, high voltages promote the full Li^+ extraction, removing the Li^+ and favoring the H^+ insertion. Our study confirms that H^+ intercalation is energetically favorable than Li^+, which may explain the cathode deterioration observed at high working voltages,[5] carrying out the complete Li^+ extraction and making the H^+ intercalation easier. Thus, the operating voltage used in cyclability experiments avoids the electrolyte decomposition, ensures the constant presence of Li^+ in the lattice, and inhibits the H^+ intercalation.

To test further the key role of stacking in proton/alkali intercalation, the H^+/Na^+ exchange was carried out for the NCO layered material. NCO shows remarkable differences with respect to LCO, principally related to the great stability of both O and P stackings. The almost invariable Li^+ accommodation in octahedral LCO sites (some T stackings have been detected) leads to a competition between Li^+ and H^+. This poor versatility of Li^+ to be placed in P sites, the H^+/Li^+ repulsion, and the distortions generated in the structure make the H^+ and Li^+ mixing energetically unfavorable in O3 structures. In contrast, our simulations have predicted the energetically favored Na^+ and H^+ presence in the same host structure, where Na^+ can be accommodated in both O and P sites. Our results show the different ability of these crystal structures to host protons, revealing that layers' stacking is an important factor. Moreover, both Na^+ and H^+ can share the same layer, suggesting that H^+/Na^+ repulsion is not as strong as H^+/Li^+ repulsion. The versatility of layered $NaTmO_2$ (Tm = transition metal) materials to alternate between different stackings has been recently observed in the O3/P3-$NaTi_{0.25}Fe_{0.25}Co_{0.25}Ni_{0.25}O_2$ layered structure during the charge/discharge of Na^+ in nonaqueous electrolytes. These alternated O/P structures for LCO were investigated, displaying energies of more than 27 meV/atom.

Experimentally, it has been proved that the H^+ by Na^+ exchange reaction on P-structures is much faster (~9 h) than the H^+ by Li^+ exchange in LCO.[16] Our computations highlight the role of the P-stacking to favor the H^+ insertion thermodynamically and kinetically. We hypothesize that the fast H^+/Na^+ exchange can be related to the stable H^+/Na^+ coexistence, which may favor the simultaneous protonation and

https://doi.org/10.1021/acs.chemmater.1c01887
Chem. Mater. 2021, 33, 6942−6954

desodiation processes. In contrast, the LCO protonation would entail first the full delithiation or the formation of the two-phase solution with lithiated and protonated regions.

In summary, the applied voltage window, the H^+/Li^+ repulsion, the stacking competition, and the experimental conditions make it possible that kinetic insertion products (solid solution LCO) are observed instead of the thermodynamic one (CoO(OH)) during cyclability experiments.

4.4. Li_xCoO_2 and Na_xCoO_2 as Cathode Materials for Aqueous Ion Batteries. Our work combined with the experimental knowledge shows that layered oxide cathode materials should not be discarded as positive electrode for aqueous electrolytes one the mere fact that be layered. Both LCO and NCO tend to accommodate H^+. Nevertheless, our computations suggest that the H^+ intercalation in LCO is only possible after the full Li^+ extraction (higher voltages are needed) or the nucleation of CoO(OH) in LCO, which is kinetically difficult. Moreover, experiments have demonstrated the slow kinetics of H^+ by Li^+ exchange in LCO under favorable conditions (acidic pH). All these pieces of evidence, together with the excellent performance of LCO in cyclability experiments, make LCO an excellent choice of cathode material in aqueous electrolytes. However, the investigations for NCO are not promising. The versatility of Na^+ to be placed in both O and P sites, the energetically favorable Na^+/H^+ co-insertion predicted by our computations, and the fast kinetics of Na^+/H^+ exchange in comparison to LCO are the drawbacks of this material in comparison to Mn oxides,[74] NASICON,[75] Prussian blue analogues,[76] and Fe phosphates,[77] typical cathode materials for ASIBs.

5. CONCLUSIONS

Using DFT calculations, we have investigated the H^+ intercalation in $ACoO_2$ ($A = Li^+$ and Na^+) layered materials to better evaluate these systems as potential positive electrode materials for ALIBs and ASIBs. The grand potential phase diagram and voltage−composition curves have been built considering different LCO and NCO phases at different orderings of protons, alkali, and vacancies. The thermodynamic analysis of this data exhibits CoO(OH) as the most stable insertion/extraction product at battery operation conditions due to the formation of interlayer hydrogen bonds. This work demonstrates, in agreement with experiments, that the H^+ by Li^+ exchange reaction is more favorable than Li^+ solid solution in the CoO_2 host. Our thermostability investigations suggest that a LCO cathode material immersed in aqueous electrolytes will favor the H^+ by Li^+ exchange reaction. Nevertheless, the simulated voltage−composition plots reveal that the voltage needed to insert the protons is higher than the experimental operation voltage, which ensures the LCO stability.

Despite the fact that the full protonated polymorph is energetically favored, the stacking competition between H^+ and Li^+ and the structural distortion provoked by H^+ insertion do not favor the mixing of both ions in the same lattice. Therefore, we postulate that the full delithiation process as the previous step of H^+ insertion or the nucleation of protonated regions is the mechanism to obtain CoO(OH). Our results suggest that the Li^+ cyclability and lack of proton insertion in LCO are the result of the slow kinetics of protonation, in agreement with the slow reaction rates observed in experimental investigations. These factors make LCO as an excellent cathode material for ALIBs.

In contrast, the H^+ intercalation has been predicted in both O- and P-type Na_xCoO_2 materials, which shows the importance of alkali elements and stackings to accommodate protons. The layered structure of the NCO cathode material has an excellent versatility to become a mixed O/P stacking, showing that Na_xCoO_2 is more prone to H^+ intercalation than $LiCoO_2$. It is thus a less promising cathode material for ASIBs.

Finally, our study shows that to be layered is not an enough reason to be discarded as cathode materials using aqueous electrolytes, even though they are much prone to thermodynamically accommodate protons. We suggest that the stacking and the operation voltage are key factors to investigate the suitability or not of a layered material as the positive electrode for aqueous ion batteries.

■ ASSOCIATED CONTENT

Supporting Information

The Supporting Information is available free of charge at https://pubs.acs.org/doi/10.1021/acs.chemmater.1c01887.

Simulated grand canonical phase diagram plots (Figures S1−S3) of $(H,Li)_xCoO_2$ and $(Na,Li)_xCoO_2$ at different pHs and alkali concentrations (PDF)

■ AUTHOR INFORMATION

Corresponding Author

Geoffroy Hautier − *Institute of Condensed Matter and Nanosciences, UCLouvain, B-1348 Louvain-la-Neuve, Belgium; Thayer School of Engineering, Dartmouth College, Hanover, New Hampshire 03755, United States;* orcid.org/0000-0003-1754-2220; Email: geoffroy.hautier@dartmouth.edu

Authors

Sergio Posada-Pérez − *Institute of Condensed Matter and Nanosciences, UCLouvain, B-1348 Louvain-la-Neuve, Belgium;* orcid.org/0000-0003-4200-4264

Gian-Marco Rignanese − *Institute of Condensed Matter and Nanosciences, UCLouvain, B-1348 Louvain-la-Neuve, Belgium;* orcid.org/0000-0002-1422-1205

Complete contact information is available at: https://pubs.acs.org/10.1021/acs.chemmater.1c01887

Notes

The authors declare no competing financial interest.

■ ACKNOWLEDGMENTS

S.P.-P., G.-M.R., and G.H. are grateful to the F.R.S.-FNRS for financial support. G.H. acknowledges the Communauté Française de Belgique for the support under Grant no. ARC 18/23-093. Computational resources were provided by the supercomputing facilities of the UCLouvain (CISM) and the Consortium des Equipements de Calcul Intensif en Fédération Wallonie-Bruxelles (CECI) funded by the Fonds de la Recherche Scientifique de Belgique (F.R.S.-FNRS) under convention no. 2.5020.11.

■ REFERENCES

(1) Manthiram, A. A Reflection on Lithium-Ion Battery Cathode Chemistry. *Nat. Commun.* **2020**, *11*, No. 1550.

(2) Xu, C.; Dai, Q.; Gaines, L.; Hu, M.; Tukker, A.; Steubing, B. Future Material Demand for Automotive Lithium-Based Batteries. *Commun. Mater.* **2020**, *1*, No. 99.

(3) Chao, D.; Zhou, W.; Xie, F.; Ye, C.; Li, H.; Jaroniec, M.; Qiao, S. Roadmap for Advanced Aqueous Batteries: From Design of Materials to Applications. *Sci. Adv.* **2020**, *6*, No. eaba4098.

(4) Miyazaki, K.; Shimada, T.; Ito, S.; Yokoyama, Y.; Fukutsuka, T.; Abe, T. Enhanced Resistance to Oxidative Decomposition of Aqueous Electrolytes for Aqueous Lithium-Ion Batteries. *Chem. Commun.* **2016**, *52*, 4979−4982.
(5) Wang, Y.; Luo, J.; Wang, C.; Xia, Y. Hybrid Aqueous Energy Storage Cells Using Activated Carbon and Lithium-Ion Intercalated Compounds. *J. Electrochem. Soc.* **2006**, *153*, No. A1425.
(6) Chen, L.; Cao, L.; Ji, X.; Hou, S.; Li, Q.; Chen, J.; Yang, C.; Eidson, N.; Wang, C. Enabling Safe Aqueous Lithium Ion Open Batteries by Suppressing Oxygen Reduction Reaction. *Nat. Commun.* **2020**, *11*, No. 2638.
(7) Li, W.; Dahn, J. R.; Wainwright, D. S. Rechargeable Lithium Batteries with Aqueous Electrolytes. *Science* **1994**, *264*, 1115−1118.
(8) Kim, H.; Hong, J.; Park, K. Y.; Kim, H.; Kim, S. W.; Kang, K. Aqueous Rechargeable Li and Na Ion Batteries. *Chem. Rev.* **2014**, *114*, 11788−11827.
(9) Bin, D.; Wang, F.; Tamirat, A. G.; Suo, L.; Wang, Y.; Wang, C.; Xia, Y. Progress in Aqueous Rechargeable Sodium-Ion Batteries. *Adv. Energy Mater.* **2018**, *8*, No. 1703008.
(10) Liu, J.; Xu, C.; Chen, Z.; Ni, S.; Shen, Z. X. Progress in Aqueous Rechargeable Batteries. *Green Energy Environ.* **2018**, *3*, 20−41.
(11) Gu, X.; Liu, J. L.; Yang, J. H.; Xiang, H. J.; Gong, X. G.; Xia, Y. Y. First-Principles Study of H+ Intercalation in Layer-Structured $LiCoO_2$. *J. Phys. Chem. C* **2011**, *115*, 12672−12676.
(12) Shu, Q.; Chen, L.; Xia, Y.; Gong, X.; Gu, X. Proton-Induced Dysfunction Mechanism of Cathodes in an Aqueous Lithium Ion Battery. *J. Phys. Chem. C* **2013**, *117*, 6929−6932.
(13) Van Der Ven, A.; Aydinol, M. K.; Ceder, G.; Kresse, G.; Hafner, J. First-Principles Investigation of Phase Stability in $LixCoO_2$. *Phys. Rev. B* **1998**, *58*, 2975−2987.
(14) Liu, Q.; Su, X.; Lei, D.; Qin, Y.; Wen, J.; Guo, F.; Wu, Y. A.; Rong, Y.; Kou, R.; Xiao, X.; Aguesse, F.; Bareño, J.; Ren, Y.; Lu, W.; Li, Y. Approaching the Capacity Limit of Lithium Cobalt Oxide in Lithium Ion Batteries via Lanthanum and Aluminium Doping. *Nat. Energy* **2018**, *3*, 936−943.
(15) Fernández-Rodriguez, J.; Hernan, L.; Morales, J.; Tirado, J. Low-Temperature Hydrothermal Transformations of $LiCoO_2$ and $HCoO_2$. *Mater. Res. Bull.* **1988**, *23*, 899−904.
(16) Medina, E. A.; Aleksandrova, I.; Karppinen, M. Proton Intercalation into Different CoO_2 Layer Matrices. *J. Solid State Chem.* **2019**, *278*, No. 120899.
(17) Zhecheva, E.; Stoyanova, R. $Li_{1-x-y}CoO_2$ Metastable Layered Phases Obtained by Acid Digestion of $LiCoO_2$ (O3). *J. Solid State Chem.* **1994**, *109*, 47−52.
(18) Gupta, R.; Manthiram, A. Chemical Extraction of Lithium from Layered $LiCoO_2$. *J. Solid State Chem.* **1996**, *121*, 483−491.
(19) Choi, J.; Alvarez, E.; Arunkumar, T. A.; Manthiram, A. Proton Insertion into Oxide Cathodes during Chemical Delithiation. *Electrochem. Solid-State Lett.* **2006**, *9*, A241.
(20) Benedek, R.; Thackeray, M. M.; Van De Walle, A. Free Energy for Protonation Reaction in Lithium-Ion Battery Cathode Materials. *Chem. Mater.* **2008**, *20*, 5485−5490.
(21) Ruffo, R.; Wessells, C.; Huggins, R. A.; Cui, Y. Electrochemical Behavior of $LiCoO_2$ as Aqueous Lithium-Ion Battery Electrodes. *Electrochem. Commun.* **2009**, *11*, 247−249.
(22) Ramanujapuram, A.; Gordon, D.; Magasinski, A.; Ward, B.; Nitta, N.; Huang, C.; Yushin, G. Degradation and Stabilization of Lithium Cobalt Oxide in Aqueous Electrolytes. *Energy Environ. Sci.* **2016**, *9*, 1841−1848.
(23) Kresse, G.; Furthmüller, J. Efficient Iterative Schemes for Ab Initio Total-Energy Calculations Using a Plane-Wave Basis Set. *Phys. Rev. B: Condens. Matter Mater. Phys.* **1996**, *54*, 11169−11186.
(24) Perdew, J. P.; Burke, K.; Ernzerhof, M. Generalized Gradient Approximation Made Simple. *Phys. Rev. Lett.* **1996**, *77*, 3865−3868.
(25) Blöchl, P. E. Projector Augmented-Wave Method. *Phys. Rev. B* **1994**, *50*, 17953−17979.
(26) Kresse, G.; Joubert, D. From Ultrasoft Pseudopotentials to the Projector Augmented-Wave Method. *Phys. Rev. B: Condens. Matter Mater. Phys.* **1999**, *59*, 1758−1775.
(27) Pack, J. D.; Monkhorst, H. J. Special Points for Brillouin-Zone Integrations—A Reply. *Phys. Rev. B* **1977**, *16*, 1748−1749.
(28) Dudarev, S.; Botton, G. Electron-Energy-Loss Spectra and the Structural Stability of Nickel Oxide: An LSDA+U Study. *Phys. Rev. B: Condens. Matter Mater. Phys.* **1998**, *57*, 1505−1509.
(29) Jain, A.; Ong, S. P.; Hautier, G.; Chen, W.; Richards, W. D.; Dacek, S.; Cholia, S.; Gunter, D.; Skinner, D.; Ceder, G.; Persson, K. A.; Jain, A.; Ong, P.; Hautier, G.; Chen, W.; Gunter, D.; Skinner, D.; Ceder, G.; Persson, K. A. Commentary: The Materials Project: A Materials Genome Approach to Accelerating Materials Innovation Commentary: The Materials Project: A Materials Genome. *APL Mater.* **2013**, *1*, No. 011002.
(30) Delmas, C.; Fouassier, C.; Hagenmuller, P. Structural Classification and Properties of the Layered Oxides. *Physica B+C* **1980**, *99*, 81−85.
(31) Mizushima, K.; Jones, P. C.; Wiseman, P. J.; Goodenough, J. B. A New Cathode Material for Batteries of High Energy Density. *Mater. Res. Bull.* **1980**, *15*, 783−789.
(32) Van Der Ven, A.; Aydinol, M. K.; Ceder, G. First-Principles Evidence for Stage Ordering in Li_x CoO_2. *J. Electrochem. Soc.* **1998**, *145*, 2149−2155.
(33) Wolverton, C.; Zunger, A. Prediction of Li Intercalation and Battery Voltages in Layered vs. Cubic Li_xCoO_2. *J. Electrochem. Soc.* **1998**, *145*, 2424−2431.
(34) Hausbrand, R.; Cherkashinin, G.; Ehrenberg, H.; Gröting, M.; Albe, K.; Hess, C.; Jaegermann, W. Fundamental Degradation Mechanisms of Layered Oxide Li-Ion Battery Cathode Materials: Methodology, Insights and Novel Approaches. *Mater. Sci. Eng., B* **2015**, *192*, 3−25.
(35) Qian, J.; Liu, L.; Yang, J.; Li, S.; Wang, X.; Zhuang, H. L.; Lu, Y. Electrochemical Surface Passivation of $LiCoO_2$ Particles at Ultrahigh Voltage and Its Applications in Lithium-Based Batteries. *Nat. Commun.* **2018**, *9*, No. 4918.
(36) Amatucci, G. G.; Tarascon, J. M.; Klein, L. C. CoO_2, the End Member of the Li_xCoO_2 Solid Solution. *J. Electrochem. Soc.* **1996**, *143*, 1114−1123.
(37) Motohashi, T.; Katsumata, Y.; Ono, T.; Kanno, R.; Karppinen, M.; Yamauchi, H. Synthesis and Properties of CoO_2, the x = 0 End Member of the Li_xCoO_2 and Na_xCoO_2 Systems. *Chem. Mater.* **2007**, *19*, 5202−5202.
(38) Meng, Y. S.; Hinuma, Y.; Ceder, G. An Investigation of the Sodium Patterning in Na_xCoO_2 ($0.5 \leq x \leq 1$) by Density Functional Theory Methods. *J. Chem. Phys.* **2008**, *128*, No. 104708.
(39) Yabuuchi, N.; Kawamoto, Y.; Hara, R.; Ishigaki, T.; Hoshikawa, A.; Yonemura, M.; Kamiyama, T.; Komaba, S. A Comparative Study of $LiCoO_2$ Polymorphs: Structural and Electrochemical Characterization of O_2-, O_3-, and O_4-Type Phases. *Inorg. Chem.* **2013**, *52*, 9131−9142.
(40) Takada, K.; Osada, M.; Izumi, F.; Sakurai, H.; Takayama-Muromachi, E.; Sasaki, T. Characterization of Sodium Cobalt Oxides Related to PB-Phase Superconductor. *Chem. Mater.* **2005**, *17*, 2034−2040.
(41) Miclau, M.; Bokinala, K.; Miclau, N. Low-Temperature Hydrothermal Synthesis of the Three-Layered Sodium Cobaltite P3-Na_xCoO_2 ($x \sim 0.60$). *Mater. Res. Bull.* **2014**, *54*, 1−5.
(42) Lei, Y.; Li, X.; Liu, L.; Ceder, G. Synthesis and Stoichiometry of Different Layered Sodium Cobalt Oxides. *Chem. Mater.* **2014**, *26*, 5288−5296.
(43) Delaplane, R. G.; Ibers, J. A.; Ferraro, J. R.; Rush, J. J. Diffraction and Spectroscopic Studies of the Cobaltic Acid System $HCoO_2$-$DCoO_2$. *J. Chem. Phys.* **1969**, *50*, 1920−1927.
(44) Toukmaji, A. Y.; Board, J. A. Ewald Summation Techniques in Perspective: A Survey. *Comput. Phys. Commun.* **1996**, *95*, 73−92.
(45) Ong, S. P.; Richards, W. D.; Jain, A.; Hautier, G.; Kocher, M.; Cholia, S.; Gunter, D.; Chevrier, V. L.; Persson, K. A.; Ceder, G. Python Materials Genomics (Pymatgen): A Robust, Open-Source Python Library for Materials Analysis. *Comput. Mater. Sci.* **2013**, *68*, 314−319.
(46) Gale, J. D. GULP: A Computer Program for the Symmetry-Adapted Simulation of Solids. *Faraday Trans.* **1997**, *93*, 629−637.

https://doi.org/10.1021/acs.chemmater.1c01887
Chem. Mater. 2021, 33, 6942−6954

(47) Gale, J. D.; Rohl, A. L. The General Utility Lattice Program (GULP). *Mol. Simul.* **2003**, *29*, 291−341.
(48) Nørskov, J. K.; Rossmeisl, J.; Logadottir, A.; Lindqvist, L.; Kitchin, J. R.; Bligaard, T.; Jónsson, H. Origin of the Overpotential for Oxygen Reduction at a Fuel-Cell Cathode. *J. Phys. Chem. B* **2004**, *108*, 17886−17892.
(49) Ong, S. P.; Jain, A.; Hautier, G.; Kang, B.; Ceder, G. Thermal Stabilities of Delithiated Olivine MPO_4 (M = Fe, Mn) Cathodes Investigated Using First Principles Calculations. *Electrochem. Commun.* **2010**, *12*, 427−430.
(50) Ong, S. P.; Chevrier, V. L.; Hautier, G.; Jain, A.; Moore, C.; Kim, S.; Ma, X.; Ceder, G. Voltage, Stability and Diffusion Barrier Differences between Sodium-Ion and Lithium-Ion Intercalation Materials. *Energy Environ. Sci.* **2011**, *4*, 3680−3688.
(51) Doe, R. E.; Persson, K. A.; Hautier, G.; Ceder, G. First Principles Study of the Li-Bi-F Phase Diagram and Bismuth Fluoride Conversion Reactions with Lithium. *Electrochem. Solid-State Lett.* **2009**, *12*, A125.
(52) Urban, A.; Seo, D. H.; Ceder, G. Computational Understanding of Li-Ion Batteries. *Npj Comput. Mater.* **2016**, *2*, No. 16002.
(53) Ong, S. P.; Wang, L.; Kang, B.; Ceder, G. Li-Fe-P-O_2 Phase Diagram from First Principles Calculations. *Chem. Mater.* **2008**, *20*, 1798−1807.
(54) Carlier, D.; Saadoune, I.; Ménétrier, M.; Delmas, C. Lithium Electrochemical Deintercalation from O_2-$LiCoO_2$. *J. Electrochem. Soc.* **2002**, *149*, No. A1310.
(55) Chang, K.; Hallstedt, B.; Music, D.; Fischer, J.; Ziebert, C.; Ulrich, S.; Seifert, H. J. Thermodynamic Description of the Layered O_3 and O_2 Structural $LiCoO_2$-CoO_2 Pseudo-Binary Systems. *CALPHAD: Comput. Coupling Phase Diagrams Thermochem.* **2013**, *41*, 6−15.
(56) Yang, J.; Liu, H.; Martens, W. N.; Frost, R. L. Synthesis and Characterization of Cobalt Hydroxide, Cobalt Oxyhydroxide, and Cobalt Oxide Nanodiscs. *J. Phys. Chem. C* **2010**, *114*, 111−119.
(57) Du, J.; Li, C.; Wang, X.; Jones, T. G. J.; Liang, H. P. Cobalt Oxyhydroxide with Highly Porous Structures as Active and Stable Phase for Efficient Water Oxidation. *Electrochim. Acta* **2019**, *303*, 231−238.
(58) Meng, Y. S.; Arroyo-De Dompablo, M. E. Recent Advances in First Principles Computational Research of Cathode Materials for Lithium-Ion Batteries. *Acc. Chem. Res.* **2013**, *46*, 1171−1180.
(59) Okumura, T.; Yamaguchi, Y.; Shikano, M.; Kobayashi, H. Correlation of Lithium Ion Distribution and X-ray Absorption near-Edge Structure in O_3- and O_2-Lithium Cobalt Oxides from First-Principle Calculation. *J. Mater. Chem.* **2012**, *22*, 17340−17348.
(60) Kaufman, J. L.; Van Der Ven, A. $NaxCoO_2$ Phase Stability and Hierarchical Orderings in the O_3/P_3 Structure Family. *Phys. Rev. Mater.* **2019**, *3*, No. 015402.
(61) Berthelot, R.; Carlier, D.; Delmas, C. Electrochemical Investigation of the P_2-Na_xCoO_2 Phase Diagram. *Nat. Mater.* **2011**, *10*, 74−80.
(62) Nayak, P. K.; Yang, L.; Brehm, W.; Adelhelm, P. From Lithium-Ion to Sodium-Ion Batteries: Advantages, Challenges, and Surprises. *Angew. Chem., Int. Ed.* **2018**, *57*, 102−120.
(63) Shibata, T.; Fukuzumi, Y.; Kobayashi, W.; Moritomo, Y. Fast Discharge Process of Layered Cobalt Oxides Due to High Na+ Diffusion. *Sci. Rep.* **2015**, *5*, No. 8−11.
(64) Hinuma, Y.; Meng, Y. S.; Ceder, G. Temperature-Concentration Phase Diagram of P_2-Na_xCoO_2 from First-Principles Calculations. *Phys. Rev. B: Condens. Matter Mater. Phys.* **2008**, *77*, No. 224111.
(65) Kubota, K.; Kumakura, S.; Yoda, Y.; Kuroki, K.; Komaba, S. Electrochemistry and Solid-State Chemistry of $NaMeO_2$ (Me = 3d Transition Metals). *Adv. Energy Mater.* **2018**, *8*, No. 1703415.
(66) Toumar, A. J.; Ong, S. P.; Richards, W. D.; Dacek, S.; Ceder, G. Vacancy Ordering in O_3-Type Layered Metal Oxide Sodium-Ion Battery Cathodes. *Phys. Rev. Appl.* **2015**, *4*, No. 064002.
(67) Kim, J. C.; Kwon, D.; Yang, J. H.; Kim, H.; Bo, S.; Wu, L.; Kim, H.; Seo, D.; Shi, T.; Wang, J.; Zhu, Y.; Ceder, G. Direct Observation of Alternating Octahedral and Prismatic Sodium Layers in O_3-Type Transition Metal Oxides. *Adv. Energy Mater.* **2020**, *10*, No. 2001151.
(68) Balsys, R. J.; Davis, R. L. The structure of $Li_{0.43}Na_{0.36}CoO_{1.96}$ using neutron powder diffraction. *Solid State Ionics* **1994**, *69*, 69−74.
(69) Guo, X.; Wang, Z.; Deng, Z.; Wang, B.; Chen, X.; Ong, S. P. Design Principles for Aqueous Na-Ion Battery Cathodes. *Chem. Mater.* **2020**, *32*, 6875−6885.
(70) Ramana, C. V.; Mauger, A.; Gendron, F.; Julien, C. M.; Zaghib, K. Study of the Li-Insertion/Extraction Process in $LiFePO_4$/$FePO_4$. *J. Power Sources* **2009**, *187*, 555−564.
(71) Chen, H.; Hautier, G.; Jain, A.; Moore, C.; Kang, B.; Doe, R.; Wu, L.; Zhu, Y.; Tang, Y.; Ceder, G. Carbonophosphates: A New Family of Cathode Materials for Li-Ion Batteries Identified Computationally. *Chem. Mater.* **2012**, *24*, 2009−2016.
(72) Malik, R.; Zhou, F.; Ceder, G. Kinetics of Non-Equilibrium Lithium Incorporation in $LiFePO_4$. *Nat. Mater.* **2011**, *10*, 587−590.
(73) Cassone, G.; Creazzo, F.; Giaquinta, P. V.; Sponer, J.; Saija, F. Ionic Diffusion and Proton Transfer in Aqueous Solutions of Alkali Metal Salts. *Phys. Chem. Chem. Phys.* **2017**, *19*, 20420−20429.
(74) Shan, X.; Charles, D. S.; Lei, Y.; Qiao, R.; Wang, G.; Yang, W.; Feygenson, M.; Su, D.; Teng, X. Bivalence Mn_5O_8 with Hydroxylated Interphase for High-Voltage Aqueous Sodium-Ion Storage. *Nat. Commun.* **2016**, *7*, No. 13370.
(75) Gao, H.; Goodenough, J. B. An Aqueous Symmetric Sodium-Ion Battery with NASICON-Structured $Na_3MnTi(PO_4)_3$. *Angew. Chem., Int. Ed.* **2016**, *55*, 12768−12772.
(76) Wessells, C. D.; Peddada, S. V.; Huggins, R. A.; Cui, Y. Nickel Hexacyanoferrate Nanoparticle Electrodes for Aqueous Sodium and Potassium Ion Batteries. *Nano Lett.* **2011**, *11*, 5421−5425.
(77) Fernández-Ropero, A. J.; Zarrabeitia, M.; Reynaud, M.; Rojo, T.; Casas-Cabanas, M. Toward Safe and Sustainable Batteries: $Na_4Fe_3(PO_4)_2P_2O_7$ as a Low-Cost Cathode for Rechargeable Aqueous Na-Ion Batteries. *J. Phys. Chem. C* **2018**, *122*, 133−142.

https://doi.org/10.1021/acs.chemmater.1c01887
Chem. Mater. 2021, 33, 6942−6954